Judd-Ofelt analysis and luminescence studies of Er3+ doped halogeno-antimonate glasses

M. Iezid, F. Goumeidane, A. Abidi, Marcel Poulain, M. Legouera, P. Syam Prasad, M. Środa, P. Venkateswara Rao

Judd-Ofelt analysis and luminescence studies of Er^{3+} doped halogeno-antimonate glasses

M. Iezid [a *] , F. Goumeidane [b], A. Abidi [c], M. Poulain [d], M. Legouera [e], P. Syam Prasad [f]

M. Środa[g], P. Venkateswara Rao[h *]

[a] *Laboratoire d'Innovation en Construction, Eco-conception et Genie Sismique (LICEGS); University Mostafa Ben Boulaid Batna 2, Algeria*

[b] *Laboratory of Active Components and Materials; Larbi Ben M'hidi University, Oum El Bouaghi, 04000, Algeria*

[c] *Laboratory of Automatics and Signals, Annaba (LASA); Badji Mokhtar University. P.O.BOX 12, 23000 Annaba, Algeria.*

[d] *Institut des Sciences Chimiques de Rennes, University Rennes 1, France*

[e] *Laboratoire de Genie Mecanique et Materiaux; University 20 Aout 1955, Skikda, Algeria*

[f] *Department of Physics, National Institute of Technology Warangal, Warangal 506004, Telangana, India*

[g] *Faculty of Material Science and Ceramics, AGH University of Science and Technology, A. Mickiewicza 30, 30-059 Kraków, Poland*

[h] *Department of Physics, The University of the West Indies, Mona Campus, Jamaica*

Abstract

This research paper emphasized on application of Judd-Ofelt's (JO) theory for low doped erbium (0.2 mol%) halogeno- antimonate based glasses with molar composition (90 –x) Sb_2O_3 - x $ZnBr_2$ - 10 NaCl (where x = 10, 20, 30 and 40 mol%). 80 Sb_2O_3 – 9.8 $ZnBr_2$ - 10 NaCl - 0.2 Er_2O_3 glass sample has low phonon energy and high refractive index is a potential candidate for luminescence applications. Differential scanning calorimetry (DSC) measurements show good thermal stability of the prepared glass samples and on the other hand density, expansion coefficient and elastic moduli were reported. Judd-Ofelt's (JO) parameter intensities Ω_2 = 3.27 X 10^{-20} cm^2, Ω_4 = 1.24 X 10^{-20} cm^2 and Ω_6 = 1.88 X 10^{-20} cm^2 were found and these values were compared with the literature. Radiative parameters such as spontaneous emission rate, branching ratio and lifetime were calculated. We focused on a high branching ratio radiative transitions $^2H_{11/2} \rightarrow {}^4I_{15/2}$ (β = 0.94) and $^4F_{9/2} \rightarrow {}^4I_{15/2}$ (β = 0.901). The overlap between absorption and emission bands is partial and stokes type shifts were presented. The gain curves were determined after calculation of absorption and stimulated emission cross sections. The infrared transmission curve of the glass matrix was

marked extrinsic absorption bands SiO and hydroxyl OH possessed high vibration energy played quenching effect for photoluminescence.

Keywords: Er^{3+} doped glass; Judd-Ofelt theory; antimonate glass; radiative properties; gain coefficient.

***Corresponding authors: pvrao54@gmail.com ; yazidmostefa@yahoo.fr**

1. Introduction

Glasses doped with trivalent lanthanides have potential photonics applications, namely optical amplifiers, sensors, colour displays and solid state lasers [1-3]. Erbium is an effective dopant due to regularly spaced $4f^n$ energy levels [4] and it is used in telecommunications for signal amplification around 1530 nm [5]. Judd-Ofelt analysis is a powerful technique for determining radiative parameters such as spontaneous emission rate, lifetime and branching ratio [6-7]. Further, certain Judd-Ofelt's spectroscopic parameters are included in the calculation of gain and quantum efficiency [8-10]. The cross section of stimulating emission is an essential factor for the choice of vitreous matrix and in this aspect the chemical composition of different glasses has been optimized [11-12]. The low phonon energy glasses are the best candidates for photoluminescence; since low phonon energy significantly allows to increase radiative transition probabilities [13], glasses like fluoro-zirconate and heavy metal oxide based glasses (HMOGs) [11, 13–15].

Antimonate glasses are part of the HMOGs exhibit good optical, photonic and mechanical properties and these glasses have a good chemical durability and low characteristic temperatures [16,17]. Moreover, antimonate based glasses are free of conventional formers (P_2O_5; B_2O_3; SiO_2) and exhibit low lanthanide solubility (Ln^{3+}) and at the limit of 0.4 mol % it became completely crystallized. The addition of conventional formers increases the solubility but reduces the phonon energy, infrared transmission and the refractive index.

The present work focuses on the application of Judd-Ofelt formalism for stable antimonate based glasses doped with erbium 80 Sb_2O_3 – 9.8 $ZnBr_2$ - 10 NaCl - 0.2 Er_2O_3. There are a few reports in literature relating to Judd-Ofelt calculations for doped antimonate glasses free of conventional formers. According to M. Legouera [18] the Sb_2O_3 - $ZnBr_2$ system generates stable glasses in a wide range where the two components act as glass formers. In the present

work, the choice of the glass matrix is based on the insertion of an additional compound (NaCl) in order to obtain a ternary system with a large glass domain, in which we will look for stable glasses. The dopant Er_2O_3 is intended for Photonics applications and this choice is supported by the low phonon energy of the antimonate and by the beneficial action of halogenated compounds ($ZnBr_2$; NaCl) which decrease the phonon density[19]. By the present analysis, we want to determine the radiative parameters of this specific glass doped at low content of trivalent erbium (0.2 mol%) and especially focused on radiative transitions; where possess a high branching ratio for determining the variation of gain coefficient related to the stimulated emission.

2. Experimental

2.1.Glass synthesis

The glass samples were prepared by melt-quenching method; using high purity chemicals $Sb_2O_3 \geq 99\%$ (Acros), $ZnBr_2 > 99\%$ (MERCK-SCHUCHARDT), NaCl > 99% (Acros), $Er_2O_3 \approx 99.9\%$ (Sigma). We have synthesized the glass matrix according to the composition (90 –x) Sb_2O_3 - x $ZnBr_2$ - 10 NaCl (where x = 10, 20, 30 and 40 mol%), and elaborated the doped glass sample at low (0.2 mol%) erbium trioxide concentration by a glass composition 80 Sb_2O_3 - 10 $ZnBr_2$ - 9.8 NaCl - 0.2 Er_2O_3 mentioned as SZNE02. The well mixed chemicals were taken in a silica crucible and brought first to around 200 ° C for 1 hour, and then to 800 ° C temperature for melting. The refining is maintained until a transparent liquid is obtained, then it is poured into brass moulds. The relaxation of the samples was carried out in an electric oven at a temperature of 250 ° C for 8 hours. After annealing, the samples are cut and polished in parallelepiped shapes with the dimensions of 10 mm × 10 mm × 3 mm.

2.2.Characterization

The density of the prepared samples was measured by the Archimedes principle with the distilled water as an immersion liquid. The DSC patterns were studied by a thermal analysis device model Q20 (TA instruments) with a heating rate 10 ° C /min and 0.1 °C sensitivity. The sample was encapsulated in hermetic aluminium's crucible; and the oven's temperature does not exceed 550 ° C, in an argon atmosphere. Incertitude is ±2 °C for glass transition and onset crystallization temperatures, and ±1 °C for peak crystallization temperature. The expansion coefficient was measured using a TMA 2940 thermo-mechanical analyser (TA instruments) with heating rate of 4 ° C/min was done between room temperature and 250 °C and the error in measuring of expansion coefficient is $\pm$ 2 X 10^{-7} K^{-1}.

The young's modulus, shear modulus and Poisson's ratio were determined by ultrasonic velocimetry with an electrical pulse generator, provides the starting signal which is connected to a piezoelectric probe (transmitter/receiver) of the Panametrics 5800 model. An acoustic coupling resin must connect to the probe and the sample in order to ensure good transmission of the ultrasonic waves. The longitudinal and transverse echoes are displayed by a Hewlett-Packard digital oscilloscope and are used to determine the time to transit of ultrasonic waves through the sample. The relative error in the values of the elastic moduli and the Poisson's ratio depends directly from the error made in reading the time τ which is estimated at $\Delta\tau$ =0.04 μs and the error made in measuring the thickness of the sample estimated at Δe = 0.02 mm. The calculation formulas are reported in our previous work [16].

The absorbance of doped sample was measured with a Perkin Elmer model spectrophotometer fitted with a TDS WB InGaAs detector at an interval between 200 nm and 2000 nm with a resolution of ± 1 nm. The emission of trivalent erbium was measured, under 378 nm excitation wavelength at room temperature by a ''Fluorolog FL3 - 22 SPEX - Jobin – Yvon'' fluorometer model and it is equipped with a 450 watt xenon arc lamp and emits radiation between 200 nm and 900 nm.

The double monochromator has two gratings of 1200 lines per mm for excitation at 250 nm but the emission one has the same number of lines at 500 nm. This configuration allows the first dual monochromator to have high stray white light rejection, and the second have optimum sensitivity in the range (300 nm – 850 nm). The samples are placed in cuvettes tilted 22.5 ° from the incident light to avoid interference between the excitation and emission light with the estimated resolution of ± 0.5 nm. Infrared transmission spectra were measured between 400 cm^{-1} and 4000 cm^{-1} using Fourier transform spectrophotometer TENSOR 37 FTIR with the 0.01 cm^{-1} accuracy and 1 cm^{-1} resolution.

3. Results and discussion

This section focused on glass matrix properties, Er^{3+} absorption spectra, refractive index determination, and finally Judd-Ofelt and luminescence analysis.

3.1.Glass matrix properties

Figure 1 represents the DSC patterns of the glass system (90 –x) Sb_2O_3 - x $ZnBr_2$ - 10 NaCl, with $10 \leq x \leq 40$ (mol.%) is used to identify the stable glass sample as a function of molar percentage of $ZnBr_2$, according to the criterion:

$$\Delta T = T_x - T_g \qquad (1)$$

T_x and T_g are the crystallization onset and glass transition temperatures [38], respectively.

Figure 2 shows clearly the monotonic decrease in stability as a function of chemical composition and 80 Sb_2O_3 - 10 $ZnBr_2$ - 10 NaCl is the most stable glass. The other physical parameters density, expansion coefficient and elastic moduli have been summarized in Table 1; which are within the limits of antimonate glasses and the corresponding formulas are given by [16], [18], [20]:

Density: $\rho = \frac{W_a}{W_a - W_b}\rho_x$ (2)

Where w_a and w_b are the weights of glass sample in air and in immersion liquid respectively; and ρ_x is the density of immersion liquid, distilled water.

Expansion coefficient: $\alpha_L = \frac{1}{L}\frac{\Delta L}{\Delta T}$ (3)

Where L is sample's length and $\Delta L/\Delta T$ is the rate of change in length per change in temperature.

The Young's and Shear modulus are given by equations (4) and (5) respectively and the Poisson's ratio is expressed by equation (6):

$$E = \frac{\rho V_T^2 (3V_L^2 - 4V_T^2)}{V_L^2 - V_T^2} \qquad (4)$$

$$G = \rho V_T^2 \qquad (5)$$

$$\eta = \frac{E}{2G} - 1 \qquad (6)$$

Where ρ is the density of glass sample; and V_L and V_T are the longitudinal and transverse ultrasonic velocities respectively.

3.2.Absorption spectra and refractive index of doped glass sample

The base glass was doped with the trivalent erbium, in order to determine its radiative properties, the dopant substitutes zinc bromide: 80 Sb_2O_3 - 9.8 $ZnBr_2$ - 10 NaCl - 0.2 Er_2O_3.

Figure 3a and 3**b** show the absorption spectrum of Er^{3+} in the antimonate matrix where the different absorption bands are marked with red arrows. **Figure 4** represents the Er^{3+} bands as a function of wavenumber (expressed in cm^{-1}) and were made from $^4I_{15/2}$ ground state, with

corrected baseline. We established the Urbach [21] plot to determine the optical gap of the doped glass sample. The optical absorption data were shown in **Figure 5**, which was used for the calculation of optical gap energy (E_p = 2.95 eV). The E_p value allowed to calculate the refractive index of doped glass according to Dimitov and Sakka formula [22]:

$$\frac{n^2-1}{n^2+2} = \sqrt{\frac{E_p}{20}} \qquad (7)$$

Where the refractive index n = 2.25 is high when compared to the conventional glasses; and it is due to the high polarizability of antimonate [16], [18] and the addition of dopant erbium oxide.

3.3.Judd-Ofelt and luminescence analysis

The experimental oscillator force is calculated from the absorbance data [23]:

$$F_{expt} = \frac{2330\, mc^2}{\pi e^2 N_0} \int \varepsilon(\nu)\, d\nu \qquad (8)$$

Where ***m*** and ***e*** are the mass and charge of the electron respectively, ***c*** is the speed of light, N_0 is the Avogadro's number and $\varepsilon(\nu)$ is the extinction coefficient which is determined with the Beer-Lambert law [24]:

$$\varepsilon(\nu) = \frac{\log\left(\frac{I_0}{I}\right)}{Cd} \qquad (9)$$

Where log (I_0 / I) absorbance measured as a function of wavenumber ν (cm^{-1}); C is the concentration of lanthanide in the sample (mol /L) and d is the thickness (cm).

Judd-Ofelt [6], [7] analysis allows the determination of the radiative parameters of a trivalent lanthanide doping a vitreous matrix. This concerns the determination of the Ω_k parameters (k= 2,4 and 6) by fitting the experimental and theoretical oscillator forces of the different absorbing transitions of a given Ln^{3+} lanthanide (except Yb^{3+}). If the fitting is validated, the parameters of Judd-Ofelt, $\boldsymbol{\Omega_k}$ are used to calculate the radiative parameters.

According to Judd-Ofelt theory the oscillator force for a transformation $aJ \rightarrow bJ'$ is expressed [6], [7]:

$$F_{cal} = F_{ed} + F_{md} = \frac{8\pi^2 mc\nu}{3h(2J+1)e^2n^2}\left(\chi_{ed}S_{ed} + \chi_{md}S_{md}\right) \qquad (10)$$

Note that χ_{ed} and χ_{md} are given by:

$$\chi_{ed} = \frac{n(n^2+2)^2}{9} \qquad (11)$$

$$\chi_{md} = n^3 \qquad (12)$$

The electric and magnetic dipole line forces are given by:

$$S_{ed}(aJ \rightarrow bJ') = e^2 \sum_{t=2,4,6} \Omega_t |\langle aJ|U^t|bJ'\rangle|^2 \qquad (13)$$

$$S_{md}(aJ \rightarrow bJ') = \frac{e^2}{4m^2c^2} |\langle aJ|L+2S|bJ'\rangle|^2 \qquad (14)$$

The probable magnetic dipole transitions are only which obey the selection rule $\Delta S = \Delta L = 0, \Delta J = 0, \pm 1$ and contributing to the oscillator force. The Judd-Ofelt parameters are obtained by least-squared fitting of the experimental values of the oscillator force using equation 8. According to Carnall et al. [25] the elements of the reduced matrix $|\langle aJ|U^t|bJ'\rangle|^2$ are invariable with respect to the change of vitreous matrix. The fitting precision is given by root mean square error:

$$RMSE = \sqrt{\frac{\sum\left(F_{cal} - F_{exp}\right)^2}{\xi - 3}} \qquad (15)$$

Such that ξ is the number of considered transitions; and note that: $\xi > 3$.

The spontaneous emission rate probability is calculated using the equation:

$$A(aJ, bJ') = A_{ed} + A_{md} = \frac{64\pi^4\nu^3}{3h(2J+1)}(\chi_{ed}S_{ed} + \chi_{md}S_{md}) \qquad (16)$$

Where A_{ed} and A_{md} are the electric and magnetic parts of spontaneous emission rate probabilities respectively. In this work, A_{md} values have been calculated from the values of LaF_3 (A'_{md}) and corrected for the refractive index difference using [26]:

$$A_{md} = \left(\frac{n}{n'}\right)^3 A'_{md} \qquad (17)$$

Where n and n' are the refractive indices of Er^{3+} doped antimonate glass and LaF_3, respectively. The branching ratio is expressed as follows:

$$\beta = A(aJ, bJ') \Big/ \sum_{bJ'} A(aJ, bJ') \qquad (18)$$

The lifetime is the inverse of the total spontaneous emission rate probability:

$$\tau = 1 \Big/ \sum_{bJ'} A(aJ, bJ') \qquad (19)$$

The cross section of stimulated emission is given by [9]:

$$\sigma(J \to J') = \frac{\lambda^4}{8\pi c n^2 \Delta\lambda_{eff}} A(J \to J') \qquad (20)$$

Where $\Delta\lambda_{eff}$ is full width at half maximum of emission peak (FWHM); and it is given by [4]:

$$\Delta\lambda_{eff} = \frac{1}{I_p} \int I(\lambda) d\lambda \qquad (21)$$

The first results of the application of the Judd-Ofelt formalism to the glass sample 80 Sb_2O_3 - 9.8 $ZnBr_2$ - 10 NaCl - 0.2 Er_2O_3 are reported in **Table 2**, in terms of barycentre wavelengths and oscillator forces; related to the absorption bands of Er^{3+} from $^4I_{15/2}$ ground state. Judd-Ofelt's method is validated with *RMSE* = 119.26*10^{-8}, and the percentage of relative error [27] is 8.12.

The relative error is obtained by the normalized RMSE [28]:

$$NRMS = Error\ \% = \frac{RMSE}{F_{\exp max} - F_{\exp min}} \qquad (22)$$

$F_{exp\ max}$ and $F_{exp\ min}$ are the maximum (hypersensitive transition) and minimum experimental oscillator forces, respectively.

Table 3 presents the Judd-Ofelt's parameters Ω_2 = 3.27 X 10^{-20} cm^2; Ω_4 = 1.24 X 10^{-20} cm^2 and Ω_6 = 1.88 X 10^{-20} cm^2, and the consecutive spectroscopic quality parameter Ω_4/Ω_6 = 0.66 ~~this value~~ is very close to the mean (Ω_4/Ω_6 = 0.7); knowing that the series of parameters is in

the order $\Omega_2 > \Omega_6 > \Omega_4$. In other words, the value of Ω_2 is lower than the average ($\Omega_{2\,ev} = 5.17 \times 10^{-20}$ cm^2) compared to the values reported in table 3; indicating that the erbium - ligand bond inserted into the antimonate matrix has the lowest degree of covalency [29] compared to other glasses.

Table 4 gives the radiative parameters of the glass sample 80 Sb_2O_3 - 9.8 $ZnBr_2$ - 10 NaCl - 0.2 Er_2O_3 such as the spontaneous emission rate *A*, the lifetime $\boldsymbol{\tau}$ and the branching ratio β. The infrared emission $^4I_{13/2} \rightarrow {}^4I_{15/2}$ has the maximum branching ratio β = 1; and the highest lifetime $\boldsymbol{\tau}$ = 1.07 ms (for the present work); this transition is essential in optical amplification for telecommunications [5]. Similarly, there are two other transitions with high branching ratios; and are within the detection limits of the fluorometer used in this study. The emissions are due to $^2H_{11/2} \rightarrow {}^4I_{15/2}$ (β = 0.94) and $^4F_{9/2} \rightarrow {}^4I_{15/2}$ (β = 0.901) and the emission spectrum (**Figure 6**) was measured at ambient temperature. We have established a Gaussian deconvolution between 500 nm and 600 nm in order to separate the $^2H_{11/2} \rightarrow {}^4I_{15/2}$ and $^3S_{3/2} \rightarrow {}^4I_{15/2}$ emissions. **Figure 7 and 8**; demonstrates the intervals of the overlap between emission and absorption cross section for the considered transitions. There is a partial overlap in the two considered cases, with the stocks type shift of emission peaks compared to the absorbances.

Figure 9 and **10** exhibits the variation of stimulated emission coefficient (gain) as a function of wavelength for different states of population inversion. The best gains correspond to the $^4F_{9/2} \rightarrow {}^4I_{15/2}$ transition; from the point of view for gain level, its flattening and minimum value of the population inversion index is $\boldsymbol{\gamma}$. However, this transition presents a positive gain starting from γ = 20 % and takes an average value of 5.5 X 10^{-20} cm^2, for total population inversion (γ = 100%). While the gains of the $^2H_{11/2} \rightarrow {}^4I_{15/2}$ transition are positive starting from γ = 40 % and admit an average value of 4 X 10^{-20} cm^2 for a complete population inversion. The curvature is less pronounced as the population inversion index increases and tends towards a flattening for γ = 100 %.

The typical stokes shift between luminescence and absorption bands testifies a notable presence of non-radiative processes, which make the overlap between the two curves relatively reduced. Non-radiative processes are of two types, intrinsic and extrinsic. The first one involves energy transfer, cross relaxation between lanthanides and the second one related to the multiphonon relaxation in the host matrix [30]. Likewise, the excessive concentration of lanthanide and the appearance of clusters influence negatively on the luminescence. In the

present case these processes are limited because the studied glass has low phonon energy and a relatively low doping level.

Figure 11 represents the infrared transmission of the matrix shows the existence of an OH group, and the SiO absorption band, mainly due to the silica crucible. The latter are real extrinsic luminescence extinguishers since the OH vibration takes place at the higher order vibration energy 3200 cm^{-1} and similarly SiO has high energy and it scales towards 1800 cm^{-1}. The OH content is estimated at around 190 ppm and is calculated according to: $Q = 30\ \alpha_{OH}$ the absorption coefficient $\boldsymbol{\alpha_{OH}}$ extracted from the infrared curve [30].

A multiphonon relaxation comprising many phonons (6 phonons) is prohibited in the antimonate matrix, on the other hand it is allowed by the vibrations of OH or SiO bonds since it requires a limited number of phonons compared to the latter. Some studies show that the presence of hydroxyl groups reduces the lifetime and efficiency of luminescence [31].The prepared glass sample has attractive qualities, a low phonon energy 602 cm^{-1} [32] and endowed with halogenated compounds ($ZnBr_2$ and NaCl) reducing the phonon density. Further the high value of the refractive index (n = 2.25) increases the probability of radiative processes.

4. Conclusion

The Judd-Ofelt analysis applied to the trivalent doped erbium antimonate based oxy-halogenated HMOGs 80 Sb_2O_3 - 9.8 $ZnBr_2$ - 10 NaCl - 0.2 Er_2O_3. DSC analysis showed that the glass matrix (90 –x) Sb_2O_3 - x $ZnBr_2$ - 10 NaCl is the most stable in the system at $10 \leq x \leq 40$ (mol.%). In addition to thermal analysis; other physical parameters density; expansion coefficient; elastic moduli and Poisson's ratio were calculated. The validity of Judd-Ofelt's method for the prepared glass sample is confirmed by positive Ω_2 value and 8.12 % for normalized root mean square error. Judd –Ofelt's (Ω_K, K= 2,4, 6) parameters take the values $\Omega_2 = 3.27 \times 10^{-20}$ cm^2; $\Omega_4 = 1.24 \times 10^{-20}$ cm^2 and $\Omega_6 = 1.88 \times 10^{-20}$ cm^2 ($\Omega_2 > \Omega_6 > \Omega_4$) are comparable to those reported in the literature.

The transitions admitting high branching ratio is $^2H_{11/2} \rightarrow {}^4I_{15/2}$ ($\beta = 0.94$) and $^4F_{9/2} \rightarrow {}^4I_{15/2}$ ($\beta = 0.901$) and are detected during luminescence measurements at room temperature around 378 nm excitation. Since the branching ratio values are greater than 50 %, the prepared glass sample will be suitable for the photonics applications. The calculated lifetimes are 39.4 µs and

117 μs and the overlap between the emission and absorbance peaks of these transitions are partial, with the stokes type shift between them. The stimulated emission gains as a function of wavelength for different states of population inversion have been calculated. The best gain is obtained for the second transition in terms of gain levels, as well as the minimum value of the population inversion coefficient which leading to a positive gain and its flattening. The infrared transmission of the glass matrix marks the presence of SiO and hydroxyl OH bonds, which are extrinsic extinguishers of luminescence.

References

[1] K. Mariselvam and J. Liu, "Judd-Ofelt analysis and visible luminescence of Sm^{3+} : MCZBP glass for reddish-orange laser and multi-colour display applications," *Solid State Sci.*, vol. 115, November 2020, pp. 106606, 2021.

[2] H. Zanane *et al.*, "Yb^{3+} and CaF_2 nanocrystallites-containing oxyfluorogermanotellurite glass-ceramics," *Opt. Mater. (Amst).*, vol. 90, pp. 108–117, 2019.

[3] A. Ichoja, S. Hashim, and S. K. Ghoshal, "Optik Judd − Ofelt calculations for spectroscopic characteristics of Dy^{3+} activated strontium magnesium borate glass," *Opt. - Int. J. Light Electron Opt.*, vol. 218, June, pp. 165001, 2020.

[4] N. Liyana, A. Rodin, and M. R. Sahar, “Erbium doped sodium magnesium boro-tellurite glass : Stability and Judd- Ofelt analysis BTNME2,” *Mater. Chem. Phys.*, vol. 216, June, pp. 177–185, 2018.

[5] P. Mandal, S. Aditya, and S. Ghosh, “Optimization of rare earth (Er^{3+}) doping level in lead zinc phosphate glass through Judd-Ofelt analysis,” *Mater. Chem. Phys.*, vol. 246, December 2019, pp. 122802, 2020.

[6] G. S. Ofelt, “Intensities of crystal spectra of rare-earth ions,” *J. Chem. Phys.*, vol. 37, no. 3, pp. 511–520, 1962.

[7] B. R. Judd, “Optical absorption intensities of rare-earth ions,” *Phys. Rev.*, vol. 127, no. 3, pp. 750, 1962.

[8] J. H. Choi, F. G. Shi, and A. Margaryan, “Novel alkaline-free Er^{3+} doped fluorophosphate glasses for broadband optical fiber lasers and amplifiers,” *J. Alloys. Comp.*, vol. 450, pp. 540–545, 2008.

[9] C. B. Layne, W. H. Lowdermilk, and M. J. Weber, “Multiphonon relaxation of rare-earth ions in oxide glasses,” *Phys. Rev. B*, vol. 16, no. 1, pp. 10, 1977.

[10] E. O. Serqueira, N. O. Dantas, A. F. G. Monte, and M. J. V Bell, “Judd Ofelt calculation of quantum efficiencies and branching ratios of Nd^{3+} doped glasses,” *J. Non. Cryst. Solids*, vol. 352, pp. 3628–3632, 2006.

[11] T. Xue, C. Huang, L. Wang, Y. Li, and Y. Liu, “Er^{3+} doped fluorozirconate glass modi fied by PbF_2 with high stimulated emission cross-section,” *Opt. Mater.*, vol. 77, pp. 117–121, 2018.

[12] A. Aydinli, S. Cenk, and A. Sennaro, “Effect of composition on the spontaneous emission probabilities , stimulated emission cross-sections and local environment of Tm^{3+} in $TeO_2 – WO_3$ glass,” *J. Lum.*, vol. 101, pp. 293–306, 2003.

[13] U. R. Rodríguez-mendoza, “Judd-Ofelt parameters of RE^{3+} doped fl uorotellurite glass (RE^{3+} : Pr^{3+} , Nd^{3+} , Sm^{3+} , Tb^{3+} , Dy^{3+} , Ho^{3+} , Er^{3+} , and Tm^{3+}),” *J. Alloys Compd.*, vol. 845, pp. 156028, 2020.

[14] S. Y. Marzouk and A. H. Hammad, “Influence of samarium ions on the structural , and optical properties of unconventional bismuth glass analyzed using the Judd – Ofelt

theory," *J. Lum.*, vol. 231, October 2020, 2021.

[15] D. Denux *et al.*, "Judd-Ofelt analysis and crystal field calculations of Er^{3+} ions in new oxyfluorogermanotellurite glasses and glass-ceramics," *Opt. Mater.*, vol. 100, December 2019, pp. 1–8, 2020.

[16] M. Iezid, M. Legouera, F. Goumeidane, M. Poulain, V. Nazabal, and R. Lebullenger, "Glass formation in the Sb_2O_3-$CdCl_2$-$SrCl_2$ ternary system," *J. Non. Cryst. Solids*, vol. 357, no. 15, pp. 2984–2988, 2011.

[17] F. Goumeidane, M. Legouera, M. Iezid, M. Poulain, V. Nazabal, and R. Lebullenger, "Synthesis and physical properties of glass in the Sb_2O_3-$PbCl_2$-MoO_3 system," *J. Non. Cryst. Solids*, vol. 357, no. 21, pp. 3572–3577, 2011.

[18] M. Legouera, P. Kostka, and M. Poulain, "Glass formation in the Sb_2O_3–$ZnBr_2$ binary system," *J. Phys. Chem. Solids*, vol. 65, no. 5, pp. 901–906, 2004.

[19] M.Iezid, F.Goumeidane, A.Abidi, N.Gherraf, M.Legouera, M.Poulain, T.Satyanarayana, P. SyamPrasad, P. VenkateswaraRao, "Spectroscopic analysis of up conversion luminescence in doped halogeno-antimonite glass," *Ceram. Int.*, vol. 44, no. 15, pp. 18060-18066, 2018.

[20] F. Goumeidane, M. Iezid, B. Melik, K. Ouannes, M. Legouera, M. Poulain, T. Satyanarayana, P. Syam Prasad, P. Venkateswara Rao, "Influence of molybdenum oxide on structural, optical and physical properties of oxychloride glasses for nonlinear optical devices," *Ceram. Int.*, vol. 43, no. 14, pp. 11305–11311, 2017.

[21] J. Tauc, "Optical properties and electronic structure of amorphous Ge and SiNo Title," *Mater. Res. Bull.*, vol. 3, no. 1, pp. 37–46, 1968.

[22] V. Dimitrov and S. Sakka, "Electronic oxide polarizability and optical basicity of simple oxides. I," *J. Appl. Phys.*, vol. 79, no. 3, pp. 1736–1740, 1996.

[23] W. T. Carnall, P. R. Fields, and K. Rajnak, "Spectral intensities of the trivalent lanthanides and actinides in solution. II. Pm^{3+}, Sm^{3+}, Eu^{3+}, Gd^{3+}, Tb^{3+}, Dy^{3+}, and Ho^{3+}," *J. Chem. Phys.*, vol. 49, no. 10, pp. 4412–4423, 1968.

[24] D. F. Swinehart, "The beer-lambert law," *J. Chem. Educ.*, vol. 39, no. 7, pp. 333, 1962.

[25] K. R. W.T. Carnall, P.R. Fields, "Electronic energy levels in the trivalent lanthanide aquo ions. I. Pr^{3+}, Nd^{3+}, Pm^{3+}, Sm^{3+}, Dy^{3+}, Ho^{3+}, Er^{3+}, and Tm^{3+}," *J. Chem. Phys.*, vol. 49, no. 10, pp. 4424 – 4442, 1968.

[26] M. J. Weber, "Probabilities for radiative and nonradiative decay of Er^{3+} in La F_3," *Phys. Rev.*, vol. 157, no. 2, pp. 262, 1967.

[27] D. Chen, Y. W. Ã, Y. Yu, E. Ma, and F. Liu, "Fluorescence and Judd – Ofelt analysis of Nd^{3+} ions in oxyfluoride glass ceramics containing CaF_2 nanocrystals," *J. Phys. Chem. Solids*, vol. 68, pp. 193–200, 2007.

[28] D. Plemenos and G. Miaoulis, *Intelligent computer graphics 2011*, vol. 441. Springer, 2012.

[29] H. Ebendor and D. Ehrt, "Tb^{+3} f - d absorption as indicator of the efect of covalency on the Judd-Ofelt Ω_2 parameter in glasses," *J. Non. Cryst. Solids*, vol. 248, pp. 247–252, 1999.

[30] T. Som and B. Karmakar, "Efficient green and red fluorescence upconversion in erbium doped new low phonon antimony glasses," *Opt. Mater. (Amst).*, vol. 31, no. 4, pp. 609–618, 2009.

[31] W. Di, X. Wang, B. Chen, S. Lu, and X. Zhao, "Effect of OH^- on the luminescent efficiency and lifetime of Tb^{3+} doped yttrium orthophosphate synthesized by solution precipitation," *J. Phys. Chem. B*, vol. 109, no. 27, pp. 13154–13158, 2005.

[32] T. Som and B. Karmakar, "Structure and properties of low-phonon antimony glasses and nano glass-ceramics in K_2O–B_2O_3–Sb_2O_3 system," *J. Non. Cryst. Solids*, vol. 356, no. 20–22, pp. 987–999, 2010.

[33] T. Som and B. Karmakar, "Nephelauxetic effect of low phonon antimony oxide glass in absorption and photoluminescence of rare-earth ions," *Spectrochim. Acta Part A Mol. Biomol. Spectrosc.*, vol. 79, no. 5, pp. 1766–1782, 2011.

[34] R. E. N. Fang, Y. MEI, G. Chao, L. ZHU, and A. LU, "Thermal stability and Judd-Ofelt analysis of optical properties of Er^{3+} doped tellurite glasses," *Trans. Nonferrous Met. Soc. China*, vol. 22, no. 8, pp. 2021–2026, 2012.

[35] Z. A. S. Mahraz, M. R. Sahar, S. K. Ghoshal, and M. R. Dousti, "Concentration

dependent luminescence quenching of Er^{3+} doped zinc boro-tellurite glass," *J. Lumin.*, vol. 144, pp. 139–145, 2013.

[36] M. S. Sajna, S. Thomas, K. A. A. Mary, C. Joseph, P. R. Biju, and N. V Unnikrishnan, "Spectroscopic properties of Er^{3+} ions in multicomponent tellurite glasses," *J. Lumin.*, vol. 159, pp. 55–65, 2015.

[37] L. R. Moorthy, M. Jayasimhadri, S. A. Saleem, and D. V. R. Murthy, "Optical properties of Er^{3+} doped alkali fluorophosphate glasses," *J. Non. Cryst. Solids*, vol. 353, no. 13–15, pp. 1392–1396, 2007.

[38] Marczewska, A., & Środa, M, "Spectroscopic and thermal study of a new glass from TeO_2 Ga_2 O_3 GeO_2 system," *J. Mol. Struct.*, vol, 1164, pp.100–108, 2018.

FIGURE CAPTIONS

Fig.1. DSC patterns of glass system (90 –x) Sb_2O_3 - x $ZnBr_2$ - 10 NaCl ($10 \leq x \leq 40$ mol.%).

Fig.2. Stability of glass matrix (90 –x) Sb_2O_3 - x $ZnBr_2$ - 10 NaCl as a function of molar percentage of $ZnBr_2$.

Fig.3a. Er^{3+} absorption bands recorded between 360 nm and 460 nm for a glass sample 80 Sb_2O_3 - 9.8 $ZnBr_2$ - 10 NaCl - 0.2 Er_2O_3.

Fig.3b. Er^{3+} absorption bands recorded between 460 nm and 1600 nm for a glass sample 80 Sb_2O_3 - 9.8 $ZnBr_2$ - 10 NaCl - 0.2 Er_2O_3.

Fig.4. Er^{3+} absorption bands as a function of wavenumber and correction of the absorbance's baseline for the sample 80 Sb_2O_3 - 9.8 $ZnBr_2$ - 10 NaCl - 0.2 Er_2O_3.

Fig.5. Urbach plot of glass sample 80 Sb_2O_3 - 9.8 $ZnBr_2$ - 10 NaCl - 0.2 Er_2O_3.

Fig.6. Er^{3+} emission spectrum (at room temperature) of sample 80 Sb_2O_3 - 9.8 $ZnBr_2$ - 10 NaCl - 0.2 Er_2O_3; at excitation wavelength λ_{ex} = 378 nm.

Fig.7. Graphs of overlap limits between absorption and emission of $^4F_{9/2}$ and $^4I_{15/2}$ levels.

Fig.8. Graphs of overlap limits between absorption and emission of $^2H_{11/2}$ and $^4I_{15/2}$ levels.

Fig.9. Variation of the stimulated emission gain coefficient versus wavelength corresponding to the transition $^4F_{9/2} \rightarrow {}^4I_{15/2}$ for different states of population inversion.

Fig.10. Variation of the stimulated emission gain coefficient versus wavelength corresponding to the transition $^2H_{11/2} \rightarrow {}^4I_{15/2}$ for different states of population inversion.

Fig.11. Infrared transmission curve of 80 Sb_2O_3 - 10 $ZnBr_2$ - 10 NaCl glass.

FIGURES

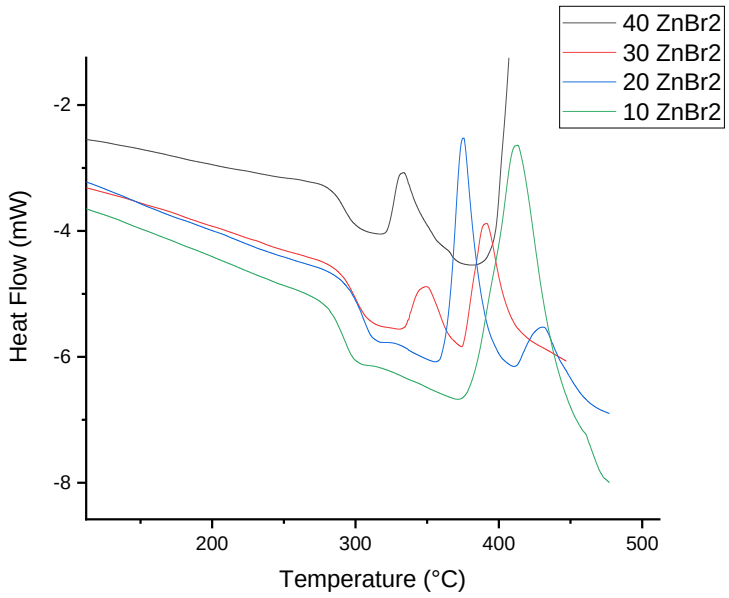

Figure 1

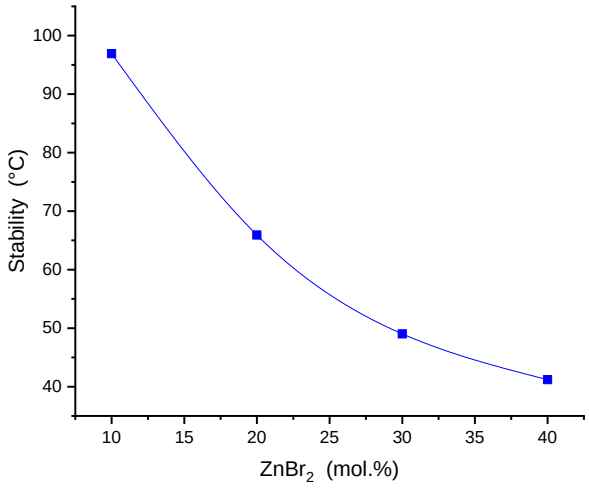

Figure 2

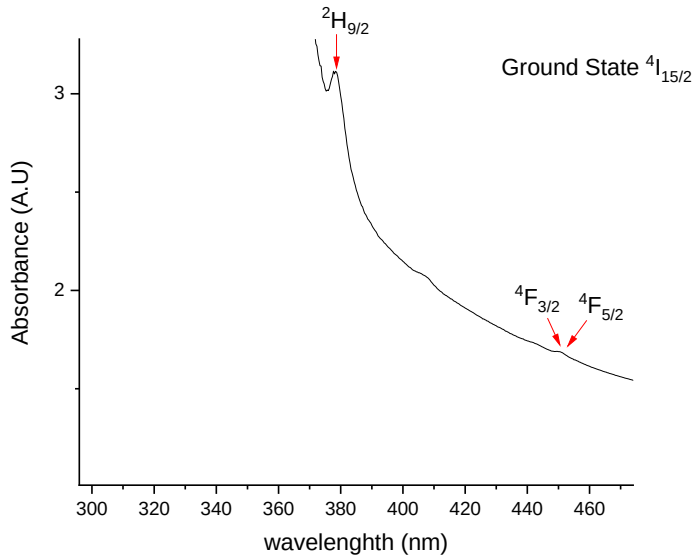

Figure 3a

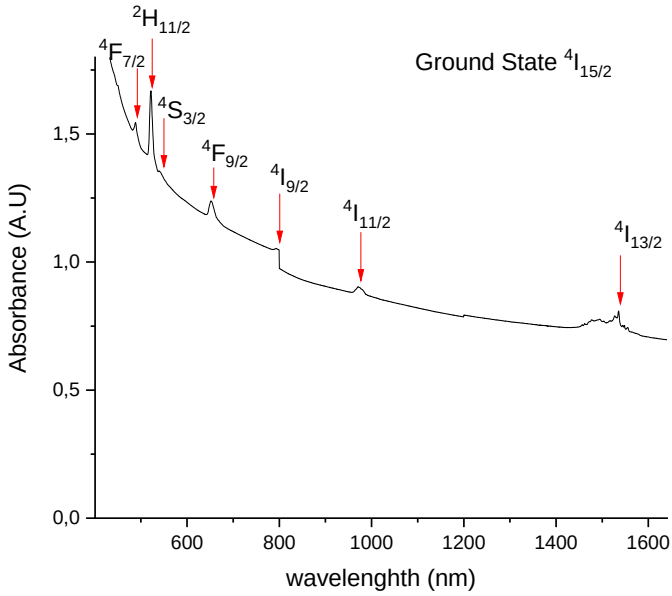

Figure 3b

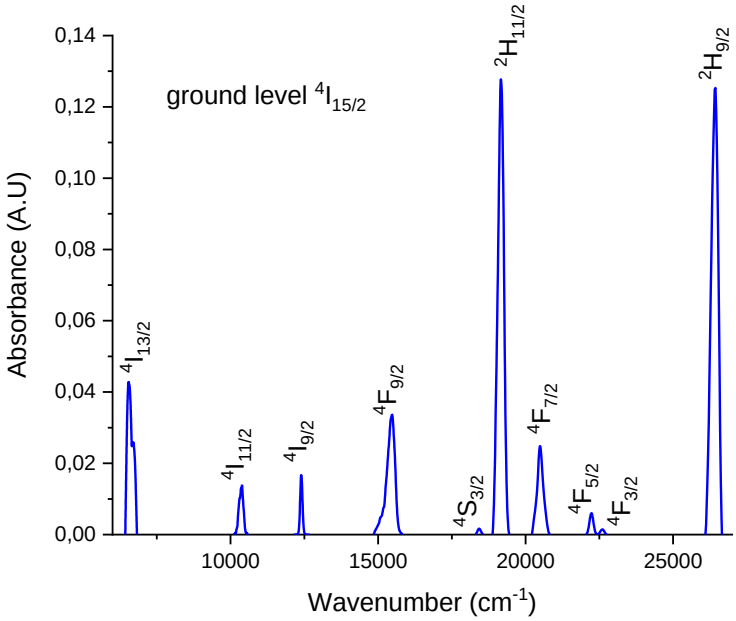

Figure 4

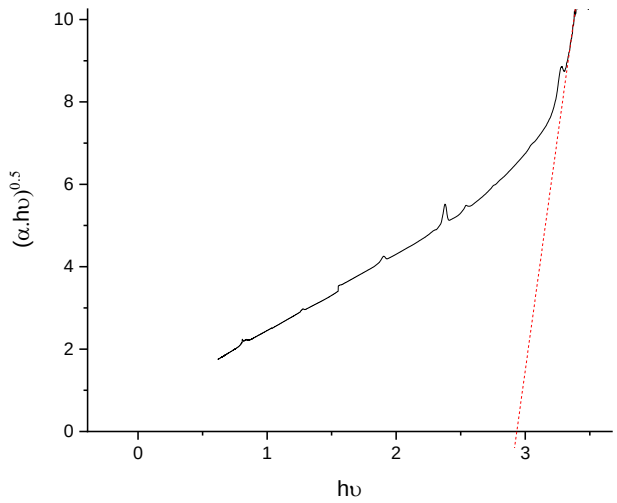

Figure 5

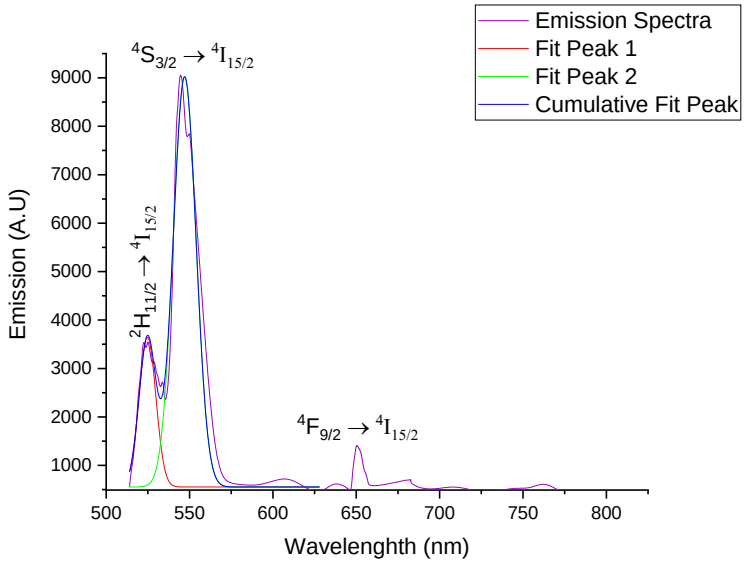

Figure 6

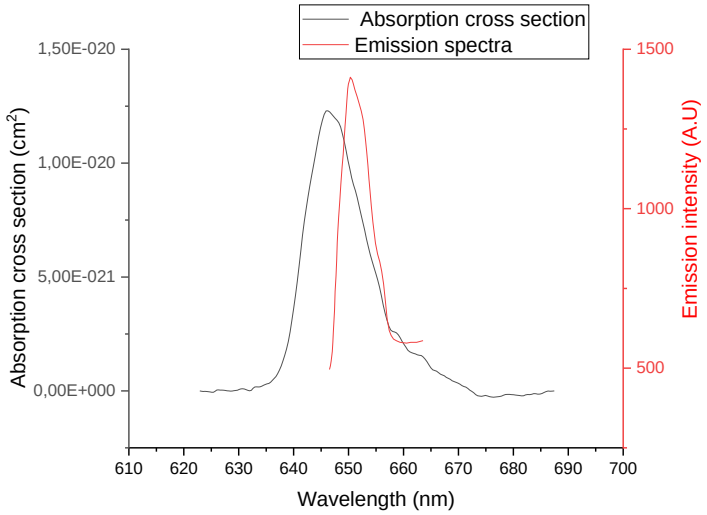

Figure 7

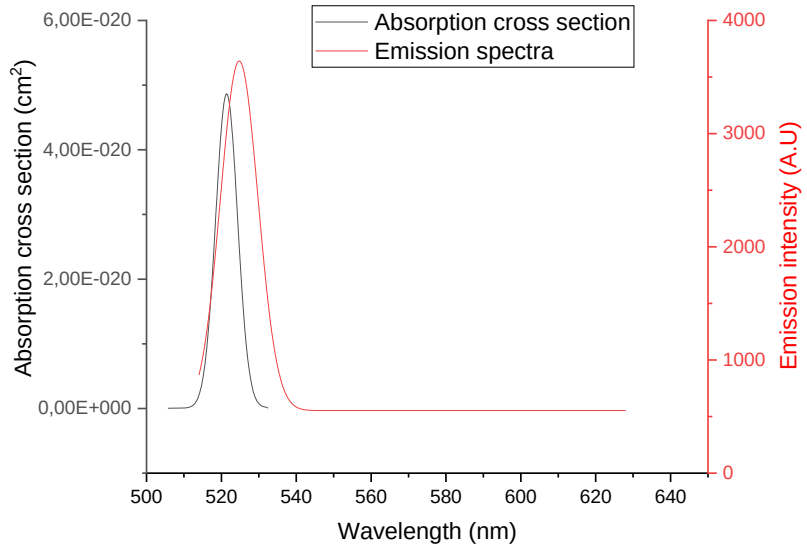

Figure 8

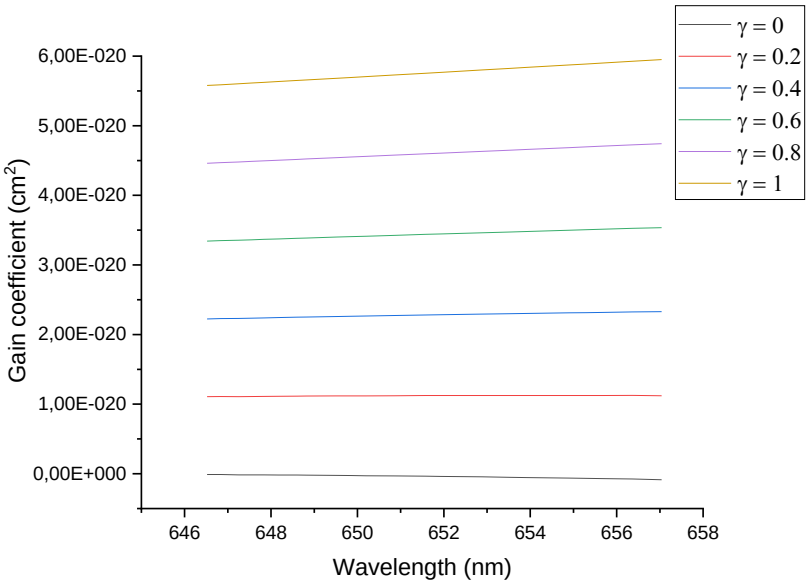

Figure 9

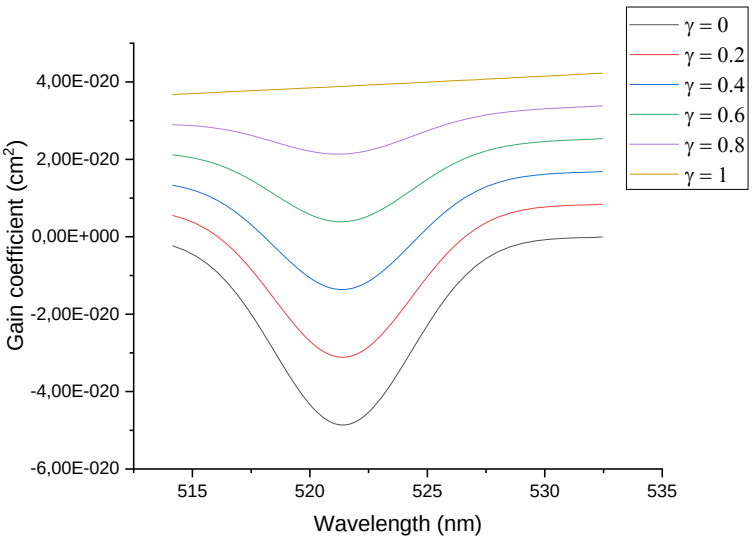

Figure 10

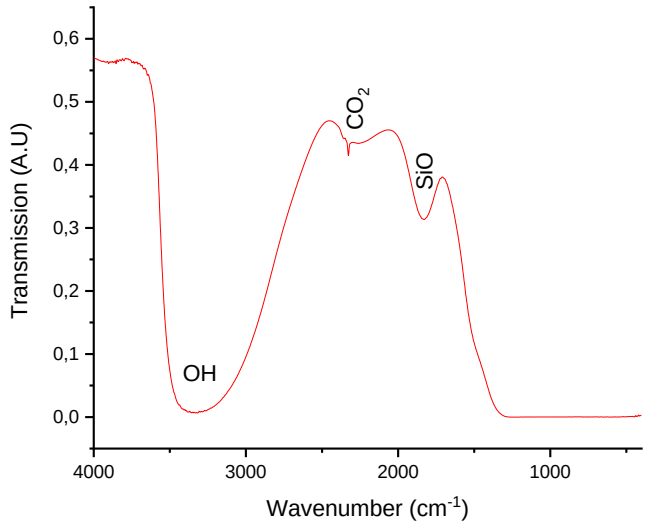

Figure 11

Tables

Table 1. Physical parameters of the glass sample 80 Sb_2O_3 - 10 $ZnBr_2$ - 10 NaCl

Density (g/cm^3)	Characteristic temperatures (°C)			Thermal expansion coefficient (10^{-6} K^{-1})	Elastic modulus and Poisson coefficient		
	T_g	T_x	T_p		E (GPa)	G (GPa)	η
4.515	279	376	413	19.92	26.24	10.64	0.2323

Table 2: Barycentre wavelengths and oscillator forces of Er^{3+} absorption bands in a glass sample 80 Sb_2O_3 - 9.8 $ZnBr_2$ - 10 NaCl - 0.2 Er_2O_3

Transition	Peak's barycenter (cm^{-1})	Oscillator line strength x 10^{-8}	
		F_{EXP}	F_{CAL}
$^4I_{15/2} \rightarrow {}^4I_{13/2}$	6624.74	446.94	389.52
$^4I_{15/2} \rightarrow {}^4I_{11/2}$	10379.53	79.4	143.75
$^4I_{15/2} \rightarrow {}^4I_{9/2}$	12629.98	25.53	49.27
$^4I_{15/2} \rightarrow {}^4F_{9/2}$	15441.06	420.87	395.35
$^4I_{15/2} \rightarrow {}^4S_{3/2}$	18424.44	12.94	128.96
$^4I_{15/2} \rightarrow {}^2H_{11/2}$	19158.37	1479.7	942.69
$^4I_{15/2} \rightarrow {}^4F_{7/2}$	20486.33	256.85	465.69
$^4I_{15/2} \rightarrow {}^4F_{5/2}$	22230.69	42.31	154.34
$^4I_{15/2} \rightarrow {}^4F_{3/2}$	22602.65	11.89	183.83
$^4I_{15/2} \rightarrow {}^2H_{9/2}$	26422.27	1163.2	1711.44
RMSE X 10^{-8}		119.26	
Error %		8.12	

Table 3: Comparison of the Judd-Ofelt parameters Ω_K (K = 2; 4; 6) and the spectroscopic quality parameter Ω_4 /Ω_6 of glass sample 80 Sb_2O_3 - 9.8 $ZnBr_2$ - 10 NaCl - 0.2 Er_2O_3 (SZNE02).

Glass system	Ω_2 (x10^{-20} cm^2)	Ω_4 (x10^{-20} cm^2)	Ω_6 (x10^{-20} cm^2)	Ω_4 /Ω_6	Trends
SZNE02 Present work	3.27	1.24	1.88	0.66	$\Omega_2 > \Omega_6 > \Omega_4$

BTNME2 [4]	8.13	1.71	2.45	0.70	$\Omega_2 > \Omega_6 > \Omega_4$
BTNME5 [4]	3.53	1.18	2.06	0.57	$\Omega_2 > \Omega_6 > \Omega_4$
TZNEr [33]	5.98	1.32	1.47	0.89	$\Omega_2 > \Omega_6 > \Omega_4$
TZNBG2 [34]	5.02	0.95	1.21	0.78	$\Omega_2 > \Omega_6 > \Omega_4$
1.5ErBT [35]	3.18	1.49	1.81	0.82	$\Omega_2 > \Omega_6 > \Omega_4$
TPBKZFEr05 [36]	7.23	1.02	1.46	0.70	$\Omega_2 > \Omega_6 > \Omega_4$
KTFP [37]	5.09	0.69	1.45	0.48	$\Omega_2 > \Omega_6 > \Omega_4$

Table 4: Radiative properties of glass sample 80 Sb_2O_3 - 9.8 ZnBr2 - 10 NaCl - 0.2 Er_2O_3

Transition	A_{ed} (s^{-1})	A_{md} (s^{-1})	A (s^{-1})	$\sum A$ (s^{-1})	τ (ms)	β
$^4I_{13/2} \rightarrow {}^4I_{15/2}$	816	120.44	937	937	1.07	1
$^4I_{11/2} \rightarrow {}^4I_{13/2}$	141	28.65	170			0.139

$^4I_{11/2} \rightarrow {}^4I_{15/2}$	1050		1050	1220	0.82	0.861
$^4I_{9/2} \rightarrow {}^4I_{11/2}$	5.44	3.05	8.49			0.00834
$^4I_{9/2} \rightarrow {}^4I_{13/2}$	399		399			0.392
$^4I_{9/2} \rightarrow {}^4I_{15/2}$	611		611	1020	0.98	0.6
$^4F_{9/2} \rightarrow {}^4I_{9/2}$	14	6.29	20.3			0.00237
$^4F_{9/2} \rightarrow {}^4I_{11/2}$	464	20.12	484			0.0566
$^4F_{9/2} \rightarrow {}^4I_{13/2}$	344		344			0.0402
$^4F_{9/2} \rightarrow {}^4I_{15/2}$	7710		7710	8850	0.117	0.901
$^4S_{3/2} \rightarrow {}^4F_{9/2}$	4.31		4.31			0.000329
$^4S_{3/2} \rightarrow {}^4I_{9/2}$	376		376			0.0287
$^4S_{3/2} \rightarrow {}^4I_{11/2}$	270		270			0.0206
$^4S_{3/2} \rightarrow {}^4I_{13/2}$	3560		3560			0.272
$^4S_{3/2} \rightarrow {}^4I_{15/2}$	8890		8890	13100	0.0763	0.679
$^2H_{11/2} \rightarrow {}^4S_{3/2}$	0.119		0.119			0.00000468
$^2H_{11/2} \rightarrow {}^4F_{9/2}$	71.6		71.6			0.00282
$^2H_{11/2} \rightarrow {}^4I_{9/2}$	401	3.11	404			0.0159
$^2H_{11/2} \rightarrow {}^4I_{11/2}$	275	22.48	298			0.0117
$^2H_{11/2} \rightarrow {}^4I_{13/2}$	553	195.8	749			0.0295
$^2H_{11/2} \rightarrow {}^4I_{15/2}$	23800			23800	25400	0.0394	0.94